



# 1 Snow depth derived from Sentinel-1 compared to in-situ 2 observations in northern Finland

3 Adriano Lemos<sup>1</sup>, Aku Riihelä<sup>1</sup>

4 <sup>1</sup> Finnish Meteorological Institute, Helsinki, Finland

5 *Correspondence to:* Adriano Lemos ([adriano.lemos@fmi.fi](mailto:adriano.lemos@fmi.fi))

## 6 Abstract

7

8 Seasonal snow in the northern regions plays an important role providing water resources for both consumption and  
9 hydropower generation. Moreover, the snow changes in northern Finland during winter impact the local agriculture,  
10 vegetation, tourism and recreational activities. In this study we estimated snow depth using an empirical methodology  
11 applied to the dual-polarisation of the Sentinel-1 synthetic aperture radar (SAR) images and compared with in situ  
12 measurements collected by automatic weather stations (AWS) in northern Finland. We applied an adapted version of the  
13 empirical methodology developed by Lievens et al. (2019) to retrieve snow depth, using Sentinel-1 constellation between  
14 2019 and 2022, and then compared to measurements from three automatic weather stations available over the same period.  
15 Overall, the Sentinel-1 snow depth retrievals were underestimated in comparison with the in-situ measurements from the  
16 automatic weather stations. We found slightly different patterns for the different years, and an overall correlation factor of  
17 0.41, and a higher correlation in the 2020–2021 season ( $R=0.52$ ). The high correlation between estimated and measured  
18 snow depth at the Inari Nellim location ( $R=0.81$ ) reinforces the potential ability to derive snow changes in regions where in  
19 situ measurements of snow are currently lacking. Further investigation is still necessary to better understand how the  
20 physical properties of the snowpack influence the backscatter response over shallow snow regions.

21



## 22 1 Introduction

23

24 Snow variations play an important role in the northern regions, providing water resources for both consumption and  
25 hydropower generation. Seasonal snow variations in northern Finland during winter impact the local agriculture, vegetation,  
26 tourism and recreational activities (Lehtonen et al., 2013; Luomaranta et al., 2019). Some regions in the Arctic are  
27 experiencing a shortening in the snow cover duration during the past decades, and future projections demonstrate an increase  
28 in the surface temperature and a continuous decrease of snow cover through time for the northern regions of Finland  
29 (Lehtonen et al., 2013; Luomaranta et al., 2019). Thus, extensive monitoring of snow depth is crucial for various purposes.

30

31 Different measurements efforts play an important role in monitoring snow depth, including the Automatic Weather Stations  
32 (AWS; Luomaranta et al., 2019), light detection and ranging (LiDAR) flights (Painter et al., 2016), and snow course  
33 measurements (Leppänen et al., 2016). The collection of these data provides valuable and accurate measurements. However,  
34 their spatiotemporally limited coverage restricts systematic monitoring. On the other hand, remote sensing techniques, such  
35 as satellite observations and modelling, are key to improve the monitoring of snow over large areas all year around (Tsang et  
36 al., 2022). Satellites equipped with passive microwave radiometry sensors, supported by the in situ measurements, have been  
37 extensively used to estimate snow water equivalent (SWE), the total water content in the snowpack, for decades (Takala et  
38 al., 2011; Pulliainen et al., 2020). However, despite their daily temporal resolution, the coarse spatial resolution  
39 (approximately 25 km by 25 km) and the dependency on the in-situ measurements still impose some limitations on the use of  
40 passive microwave radiometry for snow cover monitoring.

41

42 Currently, several studies in shallow snow regions, where snow thickness is lower than 1 m, make use of the synthetic  
43 aperture radar (SAR) measurements in the Ku-band ( $\sim 12 - 18$  GHz), as well as the Ka-band ( $\sim 26.5 - 40$  GHz), as these  
44 frequencies are more sensitive to snow pack changes. However, the exact knowledge of the penetration depth of the SAR  
45 signal in the snow pack still remains unknown and dependent on assumptions due to the snowpack characteristics, hindering  
46 accurate assessments (Tsang et al., 2022; Jutila and Hass, 2023).

47

48 The use of Interferometric Synthetic Aperture Radar (InSAR) technique using the L-band ( $\sim 1 - 2$  GHz) has shown promise,  
49 as it operates at lower frequencies and is less affected by the presence of vegetation and dry snow (Ruiz et al., 2022).  
50 However, the lack of freely available data makes its use more difficult. Future missions, such as the Radar Observing System  
51 for Europe in L-band (ROSE-L), as well as the NASA-ISRO Synthetic Aperture Radar (NISAR), will provide freely  
52 available L-band data worldwide, improving our understanding of snow changes and improving its monitoring capabilities.

53

54 The C-band backscatter measurements are widely used in several applications in the cryosphere. More specifically in the  
55 context of snow research, previous studies explore the application of the SAR images to provide information of dry snow



56 accumulation (Bernier and Fortin, 1998), and evaluation of snowmelt dynamics in the alpine regions (Marin et al., 2020).  
57 Despite some limitations, the use of the C-band (5 – 6 GHz) synthetic aperture radar images have demonstrated the ability to  
58 estimate snow depth and provide valuable information about snow depth variations using the Sentinel-1 (S1) constellation  
59 (Lievens et al., 2019, 2022). They demonstrated the sensitivity of the co- and cross-polarised backscatter observations from  
60 the Sentinel-1 satellites to estimate snow depth over mountainous regions in the Northern Hemisphere, where the snow  
61 thickness exceeds 1 m. These findings open the potential and significance of the use of the Sentinel-1 SAR images archive to  
62 estimate snow depth variation.

63

64 Snow depth estimates with high spatio-temporal resolution can improve our understanding of seasonal snow mass in  
65 complex access areas. Thus, the objective of this study is to expand the use of the empirical methodology applied to  
66 synthetic aperture radar images (Lievens et al., 2019) to estimate seasonal snow depth variations over shallow snow regions,  
67 in northern Finland. The findings will then be compared with in situ measurements collected by automatic weather stations  
68 (AWS) in the same area.

69

70

## 71 **2 Data and methods**

72

### 73 **Study Area**

74

75 The study area is located in the northern region of Finland, between the latitudes 68.3° and 69.3°N (Figure 1). The study area  
76 has a relatively flat topography, ranging approximately between 100 m to 500 m in elevation. The snow depth (SD)  
77 fluctuation is influenced by the variation of the local surface air temperature and precipitation (Luomaranta et al., 2019). In  
78 the northern part from 1961–2014 the average snow depth during winter was 82.7 cm, and maximum snow depth reached  
79 121.5 cm in 2000 (Luomaranta et al., 2019). Due to its proximity, the temperature variations in Northern Finland have a  
80 strong influence of the Arctic Ocean (Aalto et al., 2016). The mean surface temperature in the north during the winter from  
81 1988–2014 was -11.1°C, and average maximum surface temperatures reached approximately -7.2°C during the winter for the  
82 same period (Luomaranta et al., 2019).

83

### 84 **Automatic weather stations**

85

86 In order to compare and evaluate the snow depth estimates derived from Sentinel-1, we used snow depth and surface air  
87 temperature measurements from three automatic weather stations (AWS), managed by the Finnish Meteorological Institute.  
88 The snow depths are measured by the Campbell Scientific SR50AH instruments mounted on the stations, and the instrument  
89 accuracy, according to the manufacturer, is approximately 1 cm. We extracted information of daily snow depth and surface



90 air temperature, spanning from 2019 to 2022, from the Finnish stations database around the Inari Lake (IL) region. The  
91 chosen the AWS's, followed by their respective locations (Figure 1), are; Inari Nellim (IN - 68.849°N, 28.399°E), Inari  
92 Kaamanen (IK - 69.141°N, 27.266°E), and Inari Angeli Lintupuoliselkä (IA - 68.903°N, 25.736°E).

93

#### 94 **Canopy cover**

95

96 We used the canopy cover from the Multi-source National Forest Inventory Raster Maps of 2021 (MS-NFI), which is  
97 processed and distributed by the Luonnonvarakeskus (Natural Resources Centre) from Finland, to evaluate the correlation  
98 with the snow depth patterns derived from Sentinel-1. The main products used to derive the canopy cover, and the other  
99 products distributed, are from the Sentinel-2A/B satellites of European Space Agency (ESA) and the Landsat 8 satellite of  
100 United States Geological Survey (USGS), the full description of the data is found in Mäkisara et al. (2022). The dataset  
101 comes in the ETRS-TM35FIN coordinate system, and the spatial resolution is posted at 16 m by 16 m. Areas affected by  
102 cloud coverage, regions outside forest land, and outside Finland are removed and disregarded (Mäkisara et al., 2022).

103

#### 104 **Sentinel-1 data**

105

106 In this study we estimated snow depth using single look complex (SLC) synthetic aperture radar images acquired in the  
107 interferometric wide swath (IW) mode from the Sentinel-1a satellite launched by the European Space Agency (ESA) in  
108 October 2014. Sentinel-1b was launched in April 2016 and ended its mission in December 2021 due to technical issues. For  
109 this reason, in the present work, we preferred to use only images acquired from Sentinel-1a, and referred from here as  
110 Sentinel-1. The Sentinel SAR instruments operate at C-band (5.405 GHz), and the IW mode has a 250 km swath and spatial  
111 resolution of 5 m in ground range and 20 m in azimuth. Each satellite from the Sentinel-1 constellation had a repeat cycle of  
112 12 days and 180 degrees orbital phasing difference. We used the dual-polarisation (VH and VV) components from 56 SAR  
113 Sentinel-1 images acquired over the same region in northern Finland. The data range acquired spans from October 2019 to  
114 May 2022 (Table S1 in the Supplementary data), and we followed the workflow described below to derive 56 snow depth  
115 maps.

116

117 In the pre-processing stage we used ESA's Sentinel Applications Platform (SNAP) software (version 8.0). We performed a  
118 standard processing routine for all the Sentinel-1 SLC IW images, including the application of the most recent orbit file,  
119 radiometric calibration, debursting and range-Doppler terrain correction using the Copernicus digital elevation model (DEM)  
120 posted to a spatial resolution grid of 30 m. In order to reduce speckle noise in the SAR measurements, we applied a moving  
121 mean filter to the data, using a kernel of 990 m by 990 m. The final pre-processed product was a time-series of stacked S1  
122 images with  $\sigma^0$  backscatter intensities in decibel (dB) for both HV and VV.

123



124 We used an adapted version of the empirical methodology developed by Lievens et al. (2019) to estimate snow depth using  
125 Sentinel-1 products (Equations 1 and 2). The algorithm utilises changes in the cross-polarized backscatter measurements of  
126 SAR images repeatedly acquired on the same location and orbit to avoid geometry distortions. We calculated the ratio  
127 between the two cross-polarised ( $\sigma_{vh}^0$  and  $\sigma_{vv}^0$ ) backscatter intensities in a pixel scale for the entire image time-series. We  
128 considered the entire region as susceptible to snow accumulation, and the snow index (SI) in the time step  $t_i$ , was calculated  
129 as described in the Equation (1). Moreover, if  $SI(t_i) < 0$ , it was considered as zero.

130

$$131 SI(t_i) = SI(t_{i-1}) + [(\sigma_{vh}^0 / \sigma_{vv}^0)(t_i) - (\sigma_{vh}^0 / \sigma_{vv}^0)(t_{i-1})] \quad (\text{Equation 1})$$

132

133 The translation to snow depth (SD), in metres, is then calculated using Equation 2.

134

$$135 SD(t_i) = \left( \frac{a}{1 - bFC(i)} \right) SI(t_i) \quad (\text{Equation 2})$$

136

137 The parameter  $a=1.1 \text{ m dB}^{-1}$  (Equation 2) is constant and was estimated using in situ measurements, minimising the mean  
138 absolute error (MAE) between the times series of the global average snow depth measurements and Sentinel-1 estimates in  
139 mountain regions (Lievens et al., 2019). The forest cover (FC) used here is the canopy cover from the Multi-source National  
140 Forest Inventory Raster Maps of 2021 (MS-NFI). As the canopy cover attenuates the backscatter from the snow, an  
141 additional parameter  $b=0.6$  (dimensionless), estimated by Lievens et al. (2019), is applied.

142

143 Errors in our snow depth estimates arise mainly through the radiometric accuracy for Sentinel-1, specified as  $\sim 1 \text{ dB}$  (Torres  
144 et al., 2012). Due to the fact we averaged all the  $\sigma^0$  images to reduce speckle, an additional  $0.5 \text{ dB}$  was considered into the  
145 overall radiometric accuracy (Torres et al., 2012). The resulting radiometric accuracy of  $1.5 \text{ dB}$ , representing  $\sim 10\text{-}15\%$  of the  
146  $\sigma^0$  signal, was used to determine the uncertainty of the snow depth measurements.

147

148

### 149 **3 Results and Discussions**

150

151 We used the Sentinel-1 dataset (Table S1) between 2019–2022 to produce up-to-date snow depth at our designated study area  
152 (Figure 1). To explore changes in snow depth over space and time, we further extracted time series of snow depth to compare  
153 them to independent measurements from the three automatic weather stations (Figure 2). Then, we show mean snow depths  
154 yearly in Figure 3. Figure 4 presents the snow depth estimates separated by canopy density intervals. Furthermore, in order



155 to evaluate the snow depth estimates from S1, the dataset was compared to the automatic weather stations in different  
156 scenarios, presented in the Figures 5 and 6.

157

158 Figure 2 displays the seasonal changes in the snow depth over three consecutive winters at the AWS sites. We observe that  
159 the snow depth estimates from S1 at the Inari Nellim location (Figure 2a) follows the seasonal variations measured by the  
160 automatic weather stations measurements, despite the underestimated values. The snow depth products derived from  
161 Sentinel-1 from the other weather stations, IK and IA (Figure 2a), also follow the seasonality of the weather stations  
162 measurements, although they exhibit an evident underestimation relative to the AWS measurements. Automatic weather  
163 stations are usually located in relatively flat and non-forested terrain, which may not accurately represent the surrounding  
164 area, susceptible to changes in e.g., forest cover and terrain. Thus, it is important to highlight the challenges when comparing  
165 observations from a point-scale measurement from the AWS's, and the grid-scale estimates from Sentinel-1 (Lievens et al.,  
166 2022). Overall, we observed clear underestimations in the shallow snow depth regions (Figure 2), in agreement with Lievens  
167 et al. (2019). Theoretically, the underestimation is possibly due to the water content in the snowpack, reflecting and  
168 absorbing the backscatter signal, as the ground temperature in the accumulation period remains approximately the same,  
169 insulated by the snow (Lievens et al., 2019; Marin et al., 2020). The mean snow depths from S1 estimates are ~20.0 cm,  
170 ~10.1 cm, and ~13.4 cm, for Inari Nellim, Inari Kaamanen, and Inari Angeli L. locations respectively (Table 1). In contrast,  
171 the mean snow depth measured by the automatic weather stations IN, IK and IA are, respectively, ~37.1 cm, ~46.9 cm, and  
172 ~44.9 cm (Table 1). We notice from Figure S1, presenting the bias evolution of the snow depth as a function of the days of  
173 the year, that the snow season onset is well estimated by the method, despite the rapid bias increase as the snow season  
174 progresses.

175

176 The maps in Figures 3 present the average snow depth along the years. Overall, we find higher mean snow depth estimates in  
177 2019–2020 (Figure 3a), following the AWS's measurements from the time series in Figure 2 during the same year.  
178 Furthermore, we noticed higher mean snow thickness over water bodies regions, reaching values over 50 cm for all the  
179 estimates along the years (Figure 3). In order to compare the snow thickness estimates from Sentinel-1, we plotted the snow  
180 depth measured in snow pits (sp1-4 in Figure 1) during a field campaign around the Inari Lake region from the 3<sup>rd</sup> to 7<sup>th</sup> of  
181 April 2022 against the estimates 6<sup>th</sup> of April 2022 from S1 (Figure S2), as this is the closest estimate to the field  
182 measurements. We observe that, in comparison with the snow pits measurements on the lake region, all the snow depth  
183 derived from S1 are overestimated (Figure S1). Moreover, visually comparing the backscatter signal from the co- and cross-  
184 polarizations, VV and VH respectively, from S1 (Figures S3 and S4), we can observe that the VV component demonstrates  
185 to be more sensitive when the lake starts freezing, around 11th November. The backscatter signal increases (Figures S3 and  
186 S4), leading to an increase in the snow depth values.

187



188 Forest areas attenuate the radar waves, scattering the emitted and the received signal from the satellite to the snow cover on  
189 the ground, and vice-versa, leading to an underestimation of the results (Lievens et. al, 2019; Tsang et al., 2022). In order to  
190 investigate the influence of the forest cover, we divided the canopy density map (Figure 4a), from Multi-source National  
191 Forest Inventory Raster Maps of 2021, into forest cover density intervals and calculated the mean snow depth for each  
192 interval yearly (Figure 4b). We observe for all the years, and overall mean, thicker snow depth values over dense vegetation  
193 and water bodies areas, where the canopy density is equal to 0% (Figure 4b). The mean snow depth from the year 2021-2022  
194 (red bars in Figure 4) presents a slight snow depth decrease where the canopy density is above 40.. For the 2019-2020 and  
195 2020-2021 years, we found thicker snow layers over denser canopy regions (orange and green bars in Figure 4b,  
196 respectively). Despite the aligned increase of snow thickness and canopy density, the estimated snow depth over the forested  
197 areas are underestimated if compared to the automatic weather stations (Figure 2). Figure 5b shows a maximum snow depth  
198 of ~57 cm (canopy density over 20%) in 2019-2020, and a maximum snow depth of ~37 cm for the remaining years. Similar  
199 results were found using L-band SAR images, showing that the snow depth variations over the forested areas are also  
200 underestimated compared to vegetation free regions (Ruiz et al., 2022). It is important to comment that we also utilised the  
201 same approach described before (Figure 4) to correlate our snow depth estimates with terrain elevation intervals. We divided  
202 the digital elevation model in intervals every 100 m, going up to its maximum (~500 m). However, we have not found any  
203 significant correlation to include in this manuscript.

204

205 In order to compare the S1 estimates and the AWS's measurements, we calculated the temporal correlation coefficients in  
206 two different scenarios (Figs. 5 and 6). In the first scenario (Sc1) we considered all the measurements at once, as well as  
207 separated AWS's locations (Figure 5). In the second scenario (Sc2), we looked at individual years separately (Figure 6).  
208 Figure 5 displays the overall correlation, Sc1, using all the 174 measurements for all the years and from the three sites. It  
209 presented a low correlation of 0.41 and a mean absolute error of ~26.1 cm (Table 2). The estimates at the Inari Nellim  
210 weather station had a high correlation of 0.81, when compared with the other locations with  $R=0.09$  and  $R=0.55$  for Inari  
211 Kaamanen and Inari Angeli locations, respectively (Figure 5). Figure 6 presents all the 174 measurements separated yearly.  
212 We observe that the year 2020–2021 had the higher correlation factor,  $R = 0.52$ , as well as the smaller mean absolute error  
213 (~15 cm; Table 2).. The years 2019–2020 and 2021–2022 presented correlation factors of 0.29 for both years, and mean  
214 absolute errors of ~38.9 cm and ~25.5 cm, respectively (Table 2).

215

216 The uncertainty in the AWS snow depth observations (~1 cm) is considerably smaller than the uncertainty of the SAR-based  
217 estimates due to radiometric noise in the SAR imagery. At the Nellim site, a considerable part of the bias between the  
218 SAR-based estimate and ground truth could be explained by the estimation uncertainty, yet the same does not hold for either  
219 Kaamanen or Angeli. We thus conclude that the observed underestimation should be considered significant in relation to the  
220 uncertainty of the estimation method.

221



222 The backscatter signal from co-polarised images in the C-band on dry snow conditions is strongly influenced by the ground  
223 underneath, and by the water content in the snowpack (Marin et al., 2020; Lievens et al., 2022). ERS and Radarsat, both in  
224 the C-band, demonstrated an increase in the co-polarised backscatter signal during the snow accumulation periods (Bernier  
225 and Fortin, 1998) and a decrease over shallow areas (Rott and Nagler, 1993). Following the same empirical hypothesis  
226 demonstrated by Lievens et al. (2019) and Lievens et al. (2022), the cross-polarised backscatter signals at C-band are more  
227 responsive to dry snow accumulation, in comparison to the backscatter influence from the ground. Lievens et al. (2019)  
228 suggest that dry snow is represented by layers of large clusters of irregular ice crystals, scattering on the snow layer  
229 interfaces. Therefore, for deep snow locations, it is expected that layered snow enhances and dominates the backscatter  
230 signal, from cross-polarised observations (Lievens, et al., 2019).

231

232 Given the considerable underestimation of snow depth over land, and conversely considerable overestimation of snow depth  
233 over lake ice, our results reinforce the idea that the EM properties of the surface underlying the shallow seasonal snowpack  
234 likely play a major role in the observable SAR backscatter. There is a clear need for dedicated studies to improve radiative  
235 transfer modelling of volume scattering of snow in order to better explain the observed behaviour, as pointed out by Lievens  
236 et al. (2019). Finally, it is worth pointing out that the backscatter ratios are converted into snow depth through empirical  
237 coefficients. While the calibration coefficients are based on a large number of data (Lievens et al., 2019), they are based on  
238 relationships observed for mountainous snow packs, and thus not necessarily valid for shallow snow packs elsewhere.  
239 Recalibration of the coefficients is not considered here due to the limited number of reference snow depth observation sites  
240 in our study area. We also point out that at Kaamanen in particular, the temporal evolution of the backscatter ratios would not  
241 have tracked the snow depth evolution even if other linear calibrations were attempted. This further points to a need for  
242 rigorous radiative transfer studies to better understand the composition of C-band SAR backscatter over seasonal shallow  
243 snowpacks.

244

245

#### 246 **4 Conclusions**

247

248 We investigated the use of co- and cross-polarised backscatter from Sentinel-1 SAR C-band images from the Sentinel-1  
249 satellite to estimate snow depth variations over the northern region of Finland from 2019 to 2022. We presented a high  
250 temporal resolution comparison between snow depth estimated from Sentinel-1 images and measurements from automatic  
251 weather stations, and correlated with canopy cover provided by Luonnonvarakeskus (Natural Resources Institute of Finland).  
252 The use of the C-band SAR to estimate snow depth over shallow snow regions presented limitations. In general, we found  
253 underestimation for all the years and locations. It is important to highlight the snow depth estimates at the Inari Nellim  
254 location, which demonstrated the best results ( $R=0.81$ ), when compared to the automatic weather station measurements at the





255 same location. Looking throughout the years, the year 2020–2021 presented better results ( $R=0.52$ ), when compared to the  
256 previous years.

257

258 We also investigated the correlation between the canopy coverage and the snow depth estimations, and we observed thicker  
259 snow depth values over dense vegetation and water bodies regions. These findings are possibly due to the high sensitivity of  
260 the VV component over freshly frozen water, increasing the backscatter significantly. We recognize that deriving shallow  
261 snow depths using C-band SAR images is still a challenge and further investigation is necessary to better understand the  
262 observed underestimation. Thanks to the effort of international space agencies, we have available currently, and will have in  
263 the near future, global coverage at high-temporal and -spatial resolution of SAR imagery. Combined with installed automatic  
264 weather stations, this opens the possibility of a wide spatial monitoring of snow variations independent of weather or solar  
265 illumination conditions. However, given the present under- and overestimations observed against reference snow depth data,  
266 we emphasise the first-order need for rigorous radiative transfer model-based studies to comprehensively understand the  
267 drivers of SAR backscatter from snowpacks.

268

269

270 *Data availability.* The dataset will be available on the METIS - Finnish Meteorological Institute Research Data repository.

271

272 *Competing interests.* The authors declare that they have no conflict of interest.

273

274 *Acknowledgements.* This work was supported by the Academy of Finland, under the project “Low orbit altimetry, albedo,  
275 and Antarctic Snow and Sea-ice Surface Roughness” (LAS3R), grant number 335986. The authors gratefully acknowledge  
276 the European Space Agency for the Copernicus Sentinel 1 data acquired from Data Hub, courtesy of the EU/ESA. The  
277 Sentinel-1 data are freely available at <https://scihub.copernicus.eu/> (last access: 01 June 2023). The authors also  
278 acknowledge Luonnonvarakeskus (Natural Resources Institute of Finland) to provide the National Forest Inventory Raster  
279 Maps of 2021, and the Finnish Meteorological Institute for the automatic weather station datasets available at  
280 <https://hav.fmi.fi> (last access: 02 February 2023).

281



## 282 References

- 283 Aalto, J., Pirinen, P., and Jylhä, K.: New gridded daily climatology of Finland: Permutation-based uncertainty estimates and  
284 temporal trends in climate, *J. Geophys. Res.*, 121, 3807–3823, <https://doi.org/10.1002/2015JD024651>, 2016.
- 285 Bernier, M. and Fortin, J. P.: The potential of time series of C-Band SAR data to monitor dry and shallow snow cover, *IEEE*  
286 *Trans. Geosci. Remote Sens.*, 36, 226–243, <https://doi.org/10.1109/36.655332>, 1998.
- 287 Lehtonen, I., Venäläinen, A., Ikonen, J., Puttonen, N., and Gregow, H.: Some features of winter climate in Northern  
288 Fennoscandia, *Ilmatieteen Laitos Rap.*, 32, 2013.
- 289 Leppänen, L., Kontu, A., Sjöblom, H., and Pulliainen, J.: Sodankylä manual snow survey program, *Geosci. Instrum.*  
290 *Methods Data Syst.*, 5, 163–179, <https://doi.org/10.5194/gi-5-163-2016>, 2016.
- 291 Lievens, H., Demuzere, M., Marshall, H. P., Reichle, R. H., Brucker, L., Brangers, I., de Rosnay, P., Dumont, M., Girotto,  
292 M., Immerzeel, W. W., Jonas, T., Kim, E. J., Koch, I., Marty, C., Saloranta, T., Schöber, J., and De Lannoy, G. J. M.: Snow  
293 depth variability in the Northern Hemisphere mountains observed from space, *Nat. Commun.*, 10,  
294 <https://doi.org/10.1038/s41467-019-12566-y>, 2019.
- 295 Lievens, H., Brangers, I., Marshall, H. P., Jonas, T., Olefs, M., and De Lannoy, G.: Sentinel-1 snow depth retrieval at  
296 sub-kilometer resolution over the European Alps, *Cryosphere*, 16, 159–177, <https://doi.org/10.5194/tc-16-159-2022>, 2022.
- 297 Luomaranta, A., Aalto, J., and Jylhä, K.: Snow cover trends in Finland over 1961–2014 based on gridded snow depth  
298 observations, *Int. J. Climatol.*, 39, 3147–3159, <https://doi.org/10.1002/joc.6007>, 2019.
- 299 Marin, C., Bertoldi, G., Premier, V., Callegari, M., Brida, C., Hürkamp, K., Tschiersch, J., Zebisch, M., and Notarnicola, C.:  
300 Use of Sentinel-1 radar observations to evaluate snowmelt dynamics in alpine regions, *The Cryosphere*, 14, 935–956,  
301 <https://doi.org/10.5194/tc-14-935-2020>, 2020.
- 302 Painter, T. H., Berisford, D. F., Boardman, J. W., Bormann, K. J., Deems, J. S., Gehrke, F., Hedrick, A., Joyce, M., Laidlaw,  
303 R., Marks, D., Mattmann, C., McGurk, B., Ramirez, P., Richardson, M., Skiles, S. M. K., Seidel, F. C., and Winstral, A.: The  
304 Airborne Snow Observatory: Fusion of scanning lidar, imaging spectrometer, and physically-based modelling for mapping  
305 snow water equivalent and snow albedo, *Remote Sens. Environ.*, 184, 139–152, <https://doi.org/10.1016/j.rse.2016.06.018>,  
306 2016.
- 307 Pulliainen, J., Luojus, K., Derksen, C., Mudryk, L., Lemmetyinen, J., Salminen, M., Ikonen, J., Takala, M., Cohen, J.,  
308 Smolander, T., and Norberg, J.: Patterns and trends of Northern Hemisphere snow mass from 1980 to 2018, *Nature*, 581,  
309 294–298, <https://doi.org/10.1038/s41586-020-2258-0>, 2020.



- 310 Ruiz, J. J., Lemmetyinen, J., Kontu, A., Tarvainen, R., Vehmas, R., Pulliainen, J., and Praks, J.: Investigation of  
311 Environmental Effects on Coherence Loss in SAR Interferometry for Snow Water Equivalent Retrieval, *IEEE Trans. Geosci.*  
312 *Remote Sens.*, 60, 1–15, <https://doi.org/10.1109/TGRS.2022.3223760>, 2022.
- 313 Takala, M., Luojus, K., Pulliainen, J., Derksen, C., Lemmetyinen, J., Kärnä, J. P., Koskinen, J., and Bojkov, B.: Estimating  
314 northern hemisphere snow water equivalent for climate research through assimilation of space-borne radiometer data and  
315 ground-based measurements, *Remote Sens. Environ.*, 115, 3517–3529, <https://doi.org/10.1016/j.rse.2011.08.014>, 2011.
- 316 Torres, R., Snoeij, P., Geudtner, D., Bibby, D., Davidson, M., Attema, E., Potin, P., Rommen, B., Floury, N., Brown, M.,  
317 Traver, I. N., Deghaye, P., Duesmann, B., Rosich, B., Miranda, N., Bruno, C., L’Abbate, M., Croci, R., Pietropaolo, A.,  
318 Rostan, F. (2012). GMES Sentinel-1 mission. *Remote Sensing of Environment*, 120, 9–24.  
319 <https://doi.org/10.1016/j.rse.2011.05.028>
- 320 Tsang, L., Durand, M., Derksen, C., Barros, A., Kang, D.-H., Lievens, H., Marshall, H.-P., Zhu, J., Johnson, J., King, J.,  
321 Lemmetyinen, J., Sandells, M., Rutter, N., Siqueira, P., Nolin, A., Osmanoglu, B., Vuyovich, C., Kim, E., Taylor, D.,  
322 Merkouriadi, I., Brucker, L., Navari, M., Dumont, M., Kelly, R., Kim, R. S., Liao, T.-H., and Xu, X.: Review Article: Global  
323 Monitoring of Snow Water Equivalent using High Frequency Radar Remote Sensing, *The Cryosphere*, 16, 3531–3573,  
324 <https://doi.org/10.5194/tc-2021-295>, 2022.

325

326



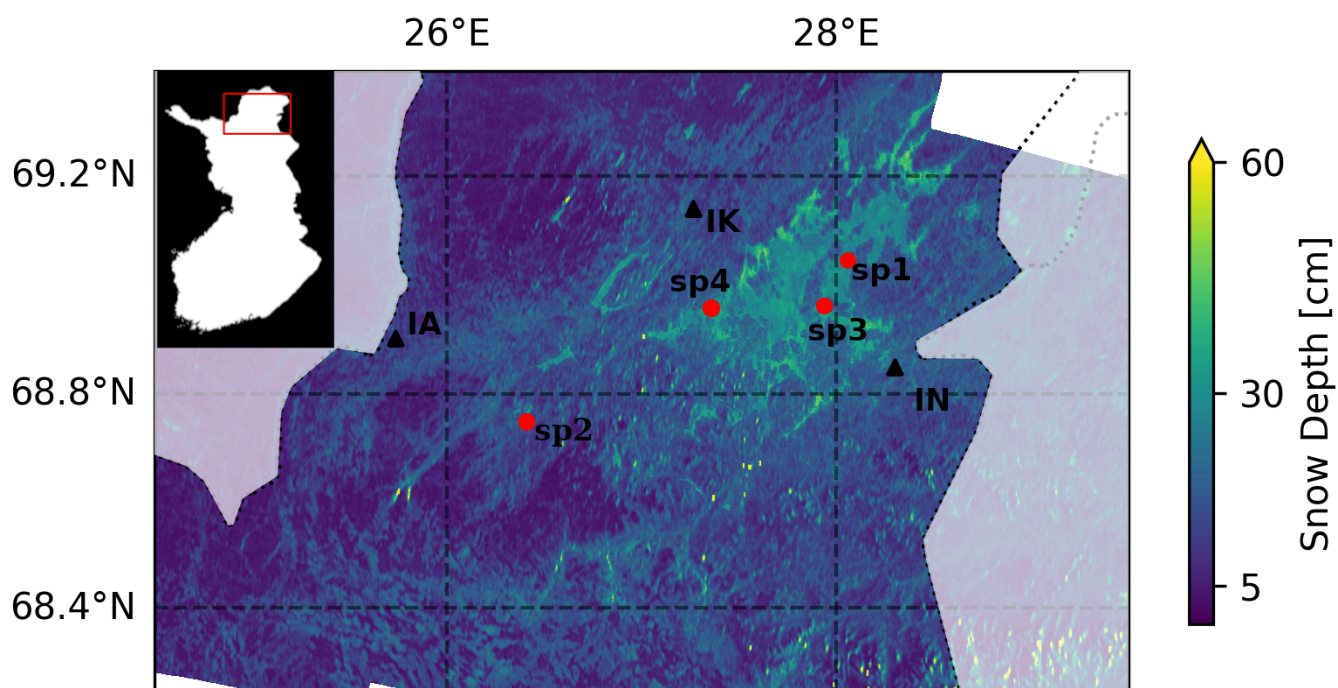
327

328 **Figures**

329

330 Figure 1: Average snow depth estimated from Sentinel-1 between 2019–2022 (between October and March). Black triangles  
331 indicate the automatic weather stations' locations; Inari Nellim (IN), Kaamanen (IK), and Angeli Lintupuoliselkä (IA),  
332 respectively. The red dots are representing the snow pits measurements (sp1–sp4). The inset figure shows the study region in  
333 Finland.

334

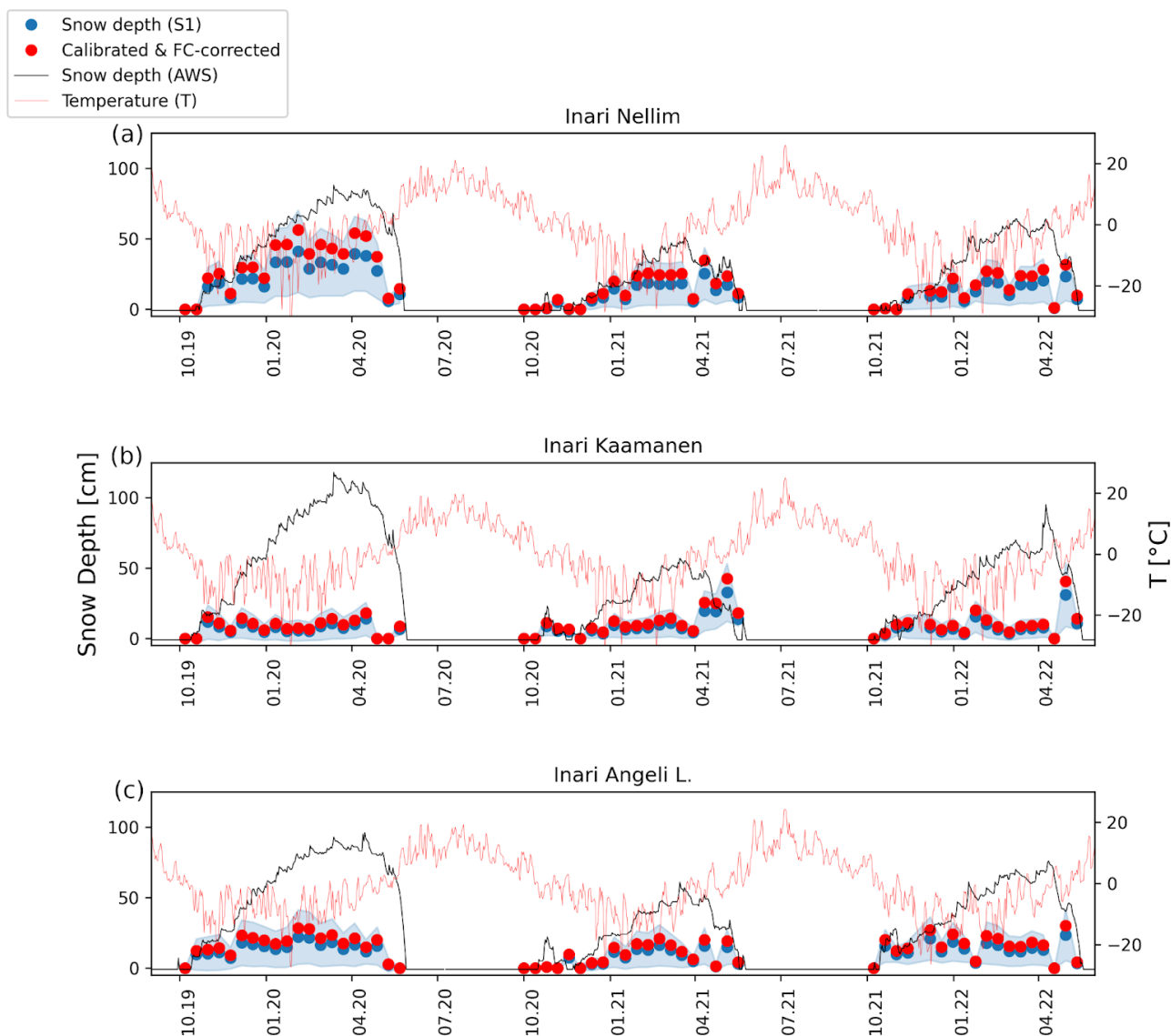


335

336



337 Figure 2: Snow depth variation between 2019 and 2022. The blues represent the snow depth variation estimated from the S1  
338 images before the correction done due the calibration and forest cover (FC) attenuation. Corrected values are represented by  
339 the red dots. The uncertainties ranges are represented by the light blue shading. On the left y-axis, the solid black line  
340 represents snow depth from the automatic weather stations and the blue dots are snow depth estimates derived by Sentinel-1.  
341 On the right y-axis, the solid red lines represent surface temperature daily averaged respectively.  
342

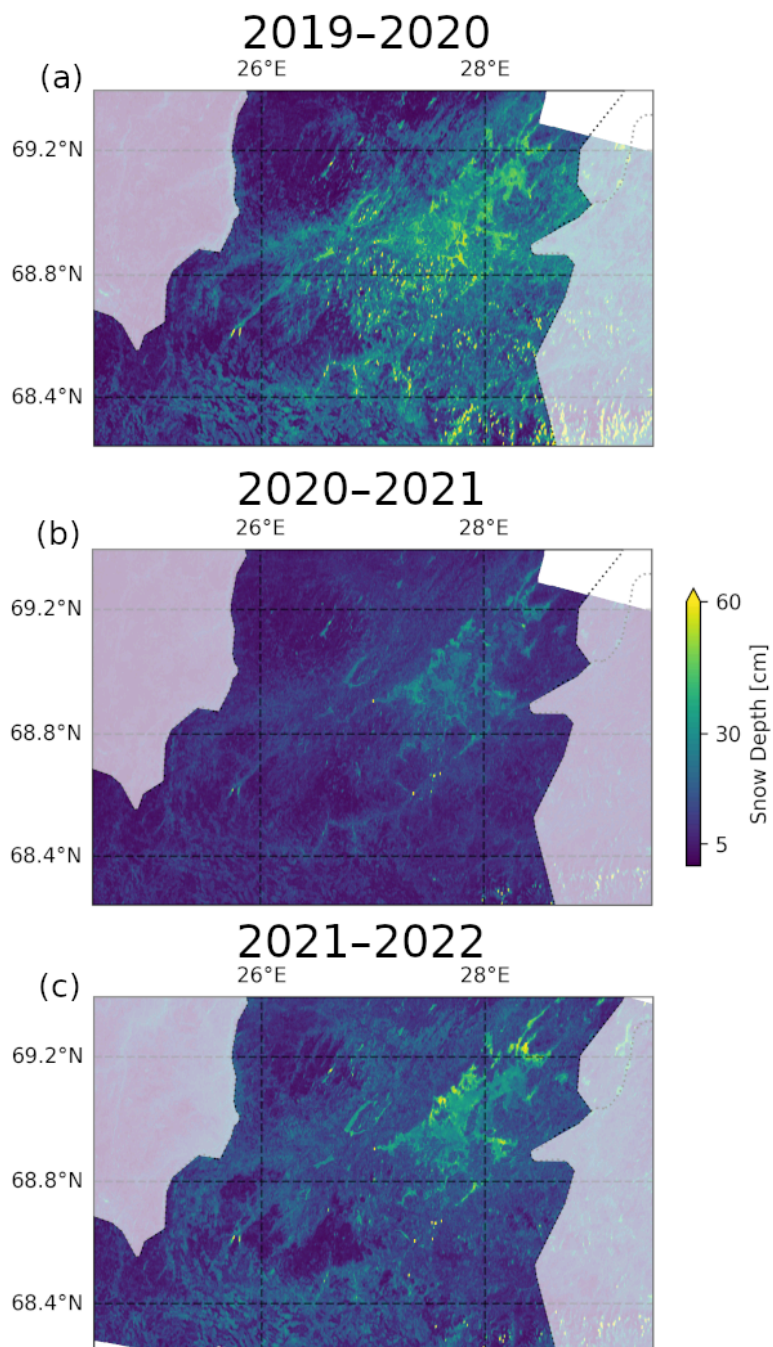


343

344



345 Figure 3: Average snow depth estimated from Sentinel-1 during the years of 2019–2020 (a), 2020–2021 (b), and 2021–2022  
346 (c), respectively.



347

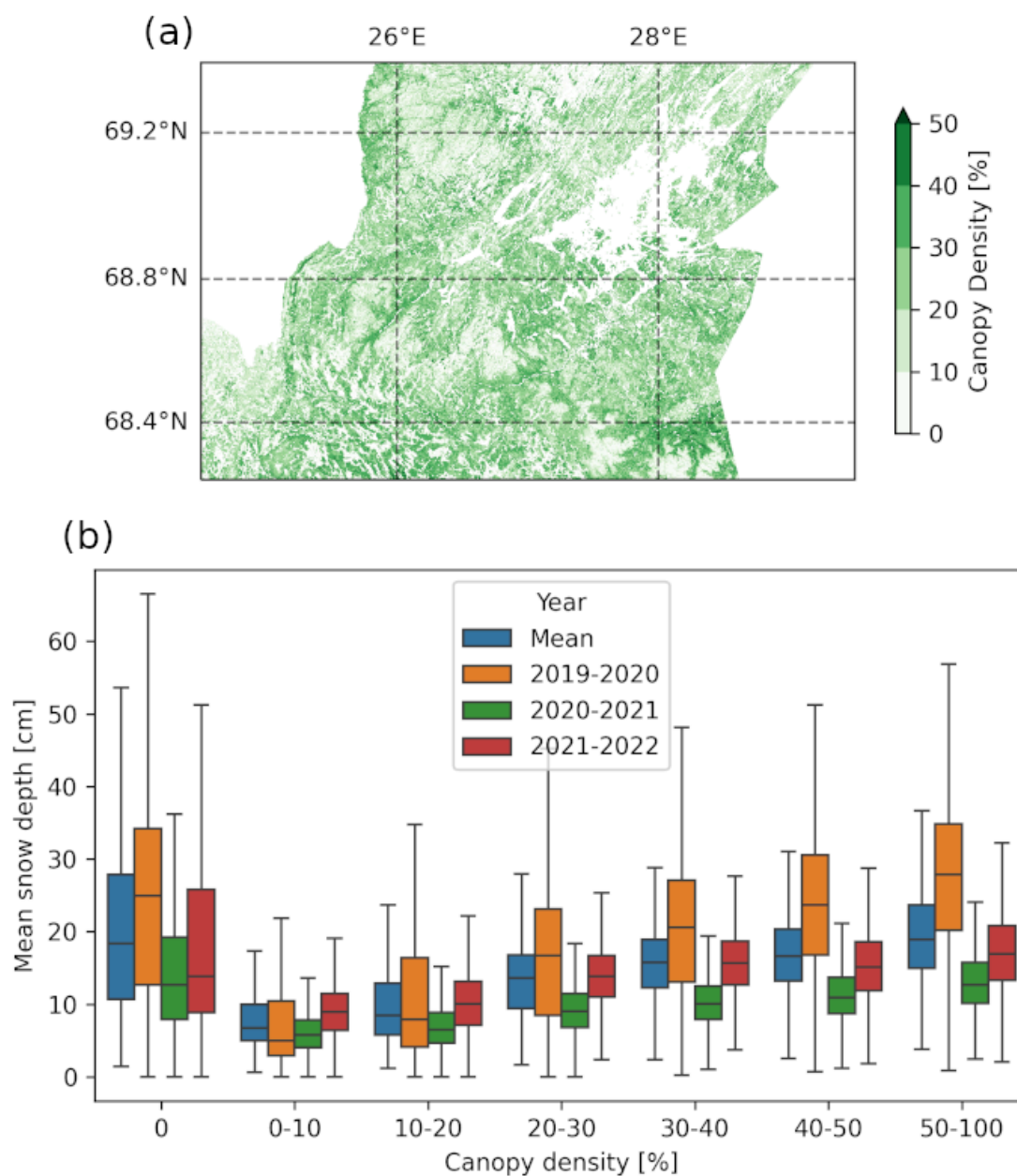
348

349





350 Figure 4: Canopy density map represented from 2021 (a). Mean snow depth separated in different canopy density intervals  
351 (b). The bottom and top of the vertical boxes represent the 25th and 75th interquartile, respectively. The solid black line  
352 inside the boxes represents the median snow depth estimate for each interval. Values outside the whiskers' extent are not  
353 shown and they are statistically considered outliers.

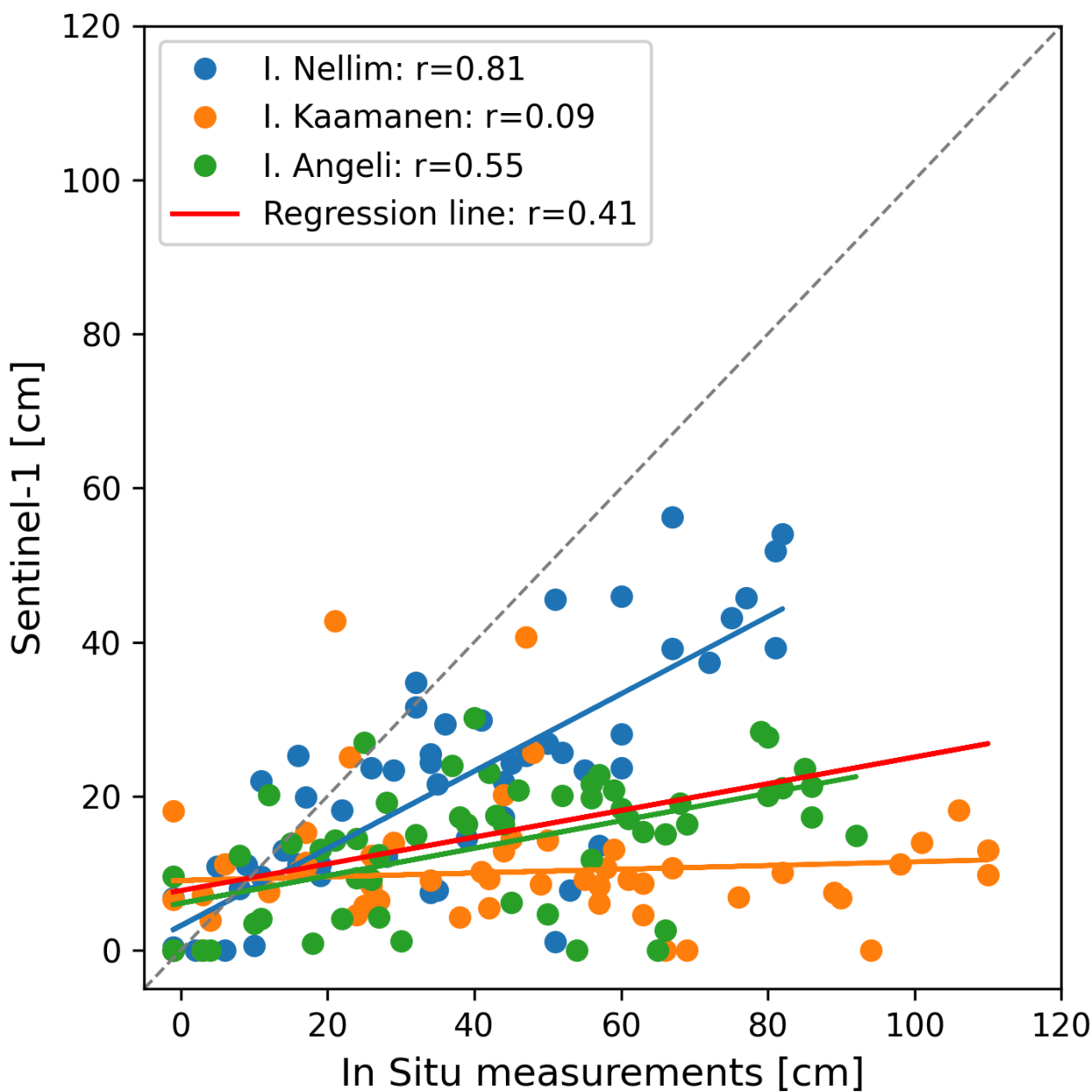


354

355



356 Figure 5: In situ measurements of snow depth compared to snow depth estimates derived from Sentinel-1. Different colours  
357 represent the different automatic weather stations, and the solid lines represent linear regressions of the dataset.



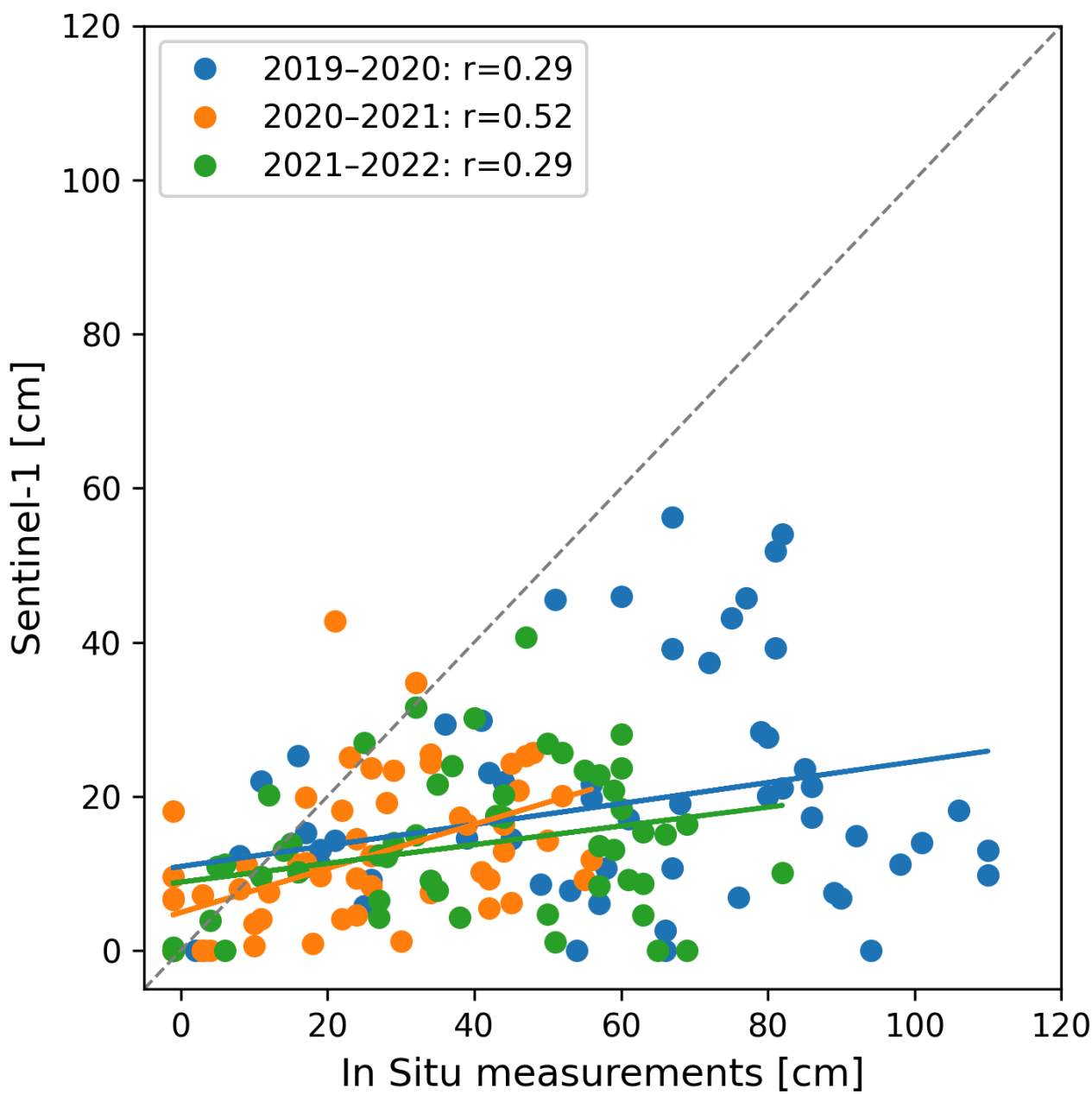
358

359





360 Figure 6: In situ measurements of snow depth compared to snow depth estimates derived from Sentinel-1. Different colours  
361 represent different years, and solid lines represent linear regression for each year.



362

363



364 Table 1: Mean snow depth values measured by the automatic weather stations (AWS) and derived from the Sentinel-1  
365 images separated by years.

366

367

	AWS mean (cm)				Sentinel-1 mean (cm)			
	2019-2020	2020-2021	2021-2022	2019-2022	2019-2020	2020-2021	2021-2022	2019-2022
Inari Nellim (IN)	53.7±1	22.1±1	35.5±1	<b>37.1±1</b>	31.0±16	13.7±8	14.8±8	<b>20.0±11</b>
Inari Kaamanen (IK)	70.9±1	28.3±1	41.6±1	<b>46.9±1</b>	8.5±7	11.6±6	10.2±7	<b>10.1±7</b>
Inari Angeli Lintupuoliselkä (IA)	61.7±1	28.1±1	44.9±1	<b>44.9±1</b>	16.3±12	8.8±6	15.4±9	<b>13.4±9</b>
Overall	<b>56.6±1</b>	<b>22.4±1</b>	<b>38.0±1</b>	<b>39.0±1</b>	<b>18.6±12</b>	<b>11.3±7</b>	<b>13.5±8</b>	<b>14.5±9</b>

368

369

370 Table 2: Mean absolute error (MAE) and root mean square error (RMSE) separated by years.

	MAE (cm)	RMSE (cm)
2019-2020	38.9	48.6
2020-2021	14.0	18.7
2021-2022	25.5	32.7
<b>2019-2022</b>	<b>26.1</b>	<b>35.6</b>

371